

Fundamentals of Bubble Transport in an Ultrasonically Assisted Separation Process

Jennifer L. Malers, Donald L. Feke
Department of Chemical Engineering
Case Western Reserve University
Cleveland, OH 44106

Abstract

The use of ultrasonic fields to induce phase separations of a dispersed solid, immiscible liquid, or gas within a suspending liquid phase has received increasing attention over the past two decades. Dissolved and entrained gases, and thus gas bubbles, have the potential to produce transport inefficiencies in closed-loop flow systems and also have the possibility of causing materials failure. Research conducted in this study investigates the applicability of the use of a resonant ultrasonic wave field to entrap and harvest gas bubbles from a surrounding liquid. By subjecting the bubbles to a standing acoustic field, their migration and coalescence can be managed, allowing for ease of removal. Current techniques for gas-liquid separations include static separators, which can be prone to fouling; vortex separators, which are not suited for low flow; and rotary separators, which tend to be mechanically complex and expensive.

This research aims to develop a fundamental understanding of the effect of forces induced by resonant ultrasonic fields on the on the entrapment and coalescence phenomena. Modeling efforts illustrate the relationship between the size of bubbles, their sphericity, acoustic field parameters (frequency and intensity), bubble placement relative to acoustic pressure antinodes, and the bubble coalescence phenomena. Experiments involving small numbers of bubbles (less than ten) are used to test the basic predictions of the model. These results support subsequent studies of the coalescence of swarms of bubbles.

Theory and Analysis of the Bubble Distortion and Entrapment Phenomena

The initial analytical portion of this research project aims to develop a fundamental understanding of the effect of buoyancy versus acoustic forces on the entrapment and coalescence phenomena. Modeling efforts illustrate the relationship between the size of bubbles, their sphericity, acoustic field parameters (frequency and intensity), bubble placement in regards to acoustic pressure antinodes, and the bubble coalescence phenomena.

Analysis of Bubble Sphericity

Performing experiments with spherical bubbles is most desirable because it allows for the least sophisticated analytical models. Pressures induced by acoustic fields can distort bubbles from a spherical shape. Therefore knowledge of this practical limit on acoustic field intensity is important. Bubble sphericity was determine based on work by Marston [1, 2], in which he used linear and inviscid theory to approximate the quadrupole projection of the acoustic radiation pressure on a compressible sphere of millimeter size. The pressure calculated in this method can be used to calculate the maximum and minimum possible radius of the deformed bubble. By allowing a maximum aspect ratio (r_{\max}/r_{\min}) of 1.1, the assumption of a spherical bubble can be used. By fixing the aspect ratio, the allowable ranges of parameters for the experimental operating conditions can be found. One of which is the

energy density in the fluid within the acoustic chamber. By determining the maximum energy density that is allowed to maintain sphericity for a bubble of a specific size, the intensity (voltage) of the acoustic field needed to fix the position of the bubble can be determined. For example, for a bubble with a 100 μm radius, the maximum average energy density that allowed the sphericity criterion to be satisfied was determined to be 0.406 J/m^3 .

Analysis of Bubble Entrapment

The physical effects referred to as body forces determine whether bubble entrapment will occur. The body forces consist of gravity, buoyancy, drag, and the primary acoustic force. Assuming the bubbles are widely spaced and there are no bubble-bubble interactions, these are the forces which determine not only the likelihood of bubble entrapment, but the position and velocity of the bubble as well. The primary acoustic force is given by Equation 1 [3], and the buoyancy and gravitational forces are given by Equation 3. The drag force is given by the Hadamard-Rybczynski formula [4] which for the gas of an air bubble in water reduces to Equation 7.

$$F_{1,ac} = 4\pi r^3 \kappa E_{ac} F \sin(2\kappa y) \quad (1)$$

$$F = \frac{\frac{1}{\hat{\sigma}^2} [3\hat{\rho} - (\frac{\kappa r}{\hat{\sigma}})^2]}{\hat{\sigma}^2 (\frac{\kappa r}{\hat{\sigma}})^6 + [3\hat{\rho} - (\frac{\kappa r}{\hat{\sigma}})^2]^2} \quad (2)$$

$$F_b = \frac{4}{3} \pi r^3 (\rho_l - \rho_g) g \quad (3)$$

$$F_d = -4\pi \mu_l r V^0 \quad (4)$$

In Equations 1-4, κ is the wavenumber, r is the radius of the bubble, E_{ac} is the average energy density in the continuous liquid phase, y is the distance of the bubble from a pressure antinode, F is the acoustic contrast factor defined in Equation 5 specifically for a gas bubble ($F = -17.7$ for the air/water system

with a bubble of 100 μm radius), $\hat{\rho} = \frac{\rho_g}{\rho_l}$, $\hat{\sigma} = \frac{c_g}{c_l}$, ρ_l and c_l are the density and speed of sound through

the continuous phase, ρ_g and c_g are the density and speed of sound through the dispersed bubble phase, and V^0 is the velocity of the moving bubble. The force balance can then be used to solve for the position and the velocity of the bubble. Figure 1 shows a position versus time graph predicted for this entrapment case, with variable initial bubble positions.

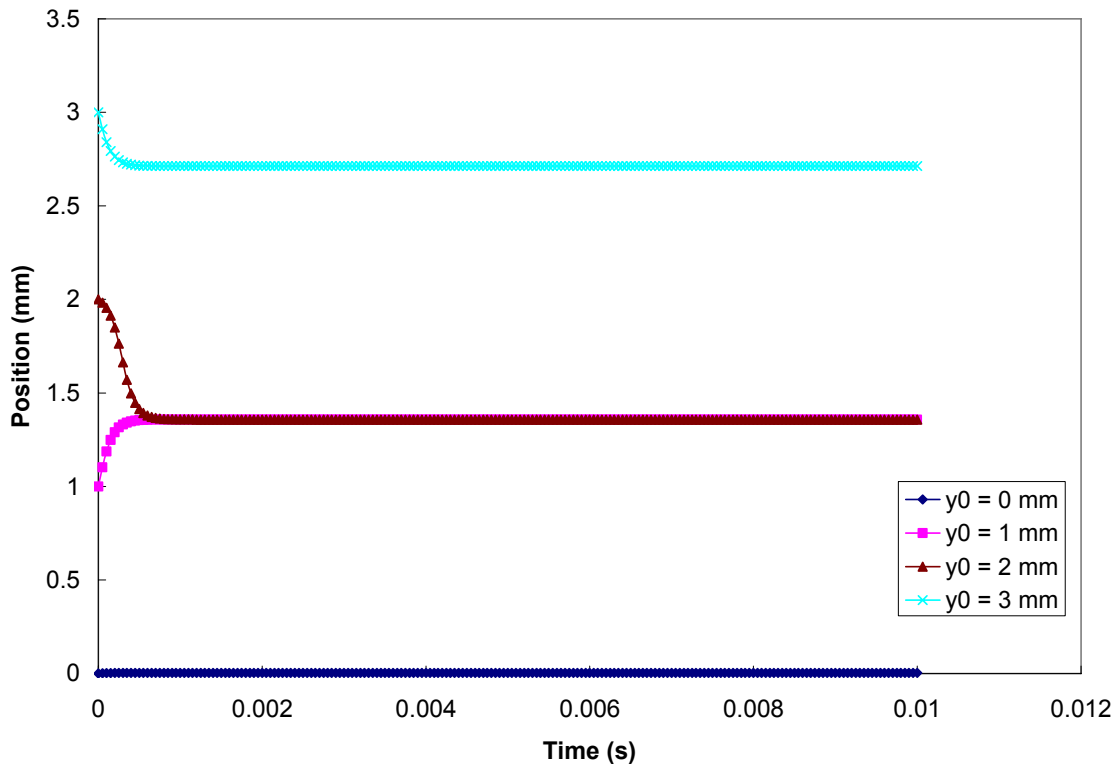


Figure 1: Position versus time graph of bubble for entrapment case, with varying initial position of the bubble with the transducer at the zero position.

In Figure 1, the bubble moves to the pressure antinode closest to its initial position. Based on a transducer operating frequency of 0.55 MHz, and thus a wavenumber of 0.271 cm, the pressure antinodes are approximated as being every 1.355 mm. The modeling shows the bubble to rest slightly above the pressure antinode, with resting positions of approximately 0.003, 1.358, and 2.713 mm shown in Figure 3. In this instance the transducer would be located at the zero position.

Experimental Setup and Data

The current acoustic chamber design being employed is a fairly simple structure. The chamber has three main sections: an acrylic chamber centerpiece, two polyethylene support structures, and a transducer and reflector. A schematic of this can be seen in Figure 2. In typical acoustic chambers, the transducers and reflectors are rigidly attached to their support structures. The disadvantage of this is that the sealant is easily fatigued which may result in leakage, and the direct connection to the support structure provides a transmission path for the acoustic energy, which can result in inefficiency in producing strong fields within the liquid itself. To counteract these issues, the chamber design used in this study incorporates a thin Latex membrane (0.02" thick) are glued around the edges of the transducer and reflector and sandwiched between the polyethylene support structures and the centerpiece. The latex membranes provide a resilient seal that withstands the vibrations of the transducer over long periods of operation [5]. The current acoustic chamber is approximately 6.3 cm wide by 6.3 cm deep with a height of 5.7 cm. The transducer (EC-64 by EDO) is 3.8 cm by 3.8 cm with a thickness of 5.08 mm. The reflector is glass and is also 3.8 cm by 3.8 cm with a thickness of 2.23 mm. The transducer and reflector are set approximately 2 cm apart within the chamber.

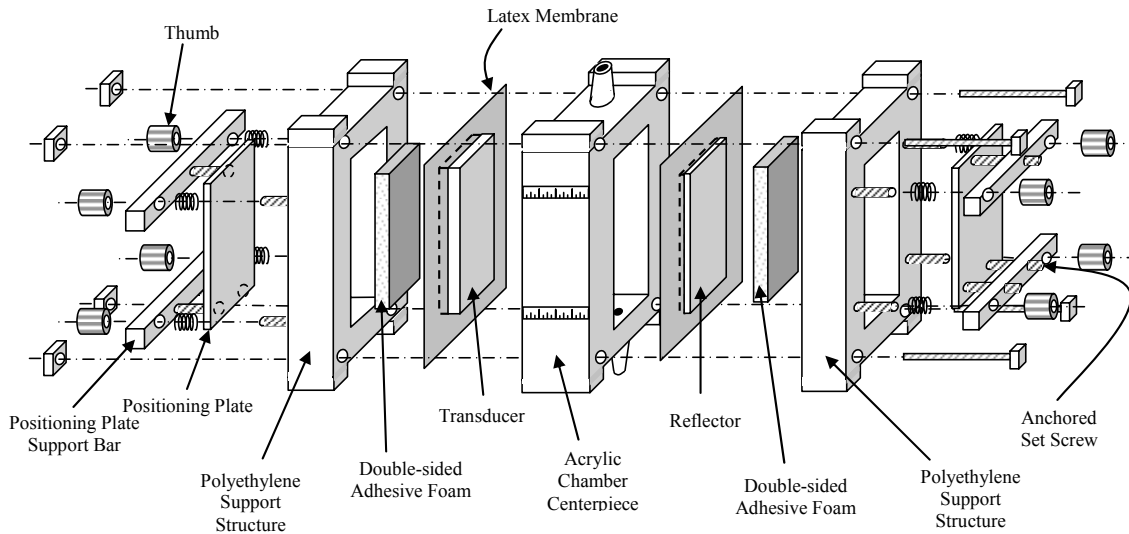


Figure 2: Schematic representation of the acoustic chamber used for experimentation. The transducer and reflector are held in place by double-sided foam attached to an adjustable positioning plate. The fluid suspension flows through the centerpiece, where, upon assembly, an airtight seal is created between the polyethylene support structures, the latex membranes glued to the transducer and reflector, and the chamber centerpiece [5].

After the chamber is pumped full of de-gassed DI water, the inlet and outlet ports are sealed, one with a rubber septum. Individual air bubbles are inserted into the acoustic chamber with a syringe which has 25s gauge needle (ID = 140 μm). Swarms of bubbles are achieved by simply de-gassing the water to a lesser extent. When running the transducer at high intensities, dissolved gas was drawn out of solution and large numbers of bubbles were formed.

Images have been obtained of the system verifying modeling efforts. Figure 3 shows a picture taken of two bubbles and the distance that they rest from each other. Again, the antinodes can be approximated as 1.355 mm apart. The image shows the bubbles to be approximately 1.32 mm apart. Although there are some intrinsic errors in the measurement process, this is a good initial indication that the system is working as predicted. The system also works well for swarms of bubbles as the bubbles readily move to pressure antinodes forming bands, which can be seen in Figure 4.

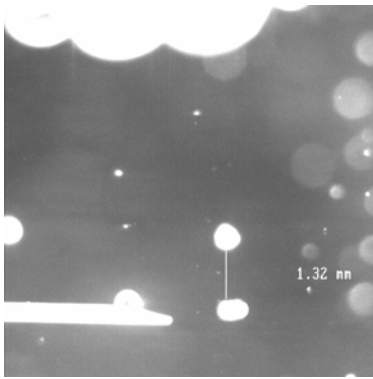


Figure 3: Image of air bubbles in water resting at pressure antinodes within the acoustic chamber. The distance between bubbles is 1.32 mm.

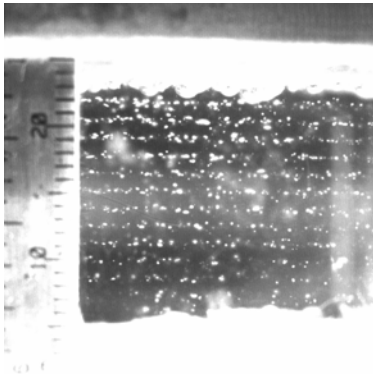


Figure 4: Entrapment of swarms of bubbles in multiple, parallel bands.

Experiments have been run for up to an hour showing that the majority of these bubbles remain trapped. Initially it was thought that there was some coalescence and subsequent release of the newly enlarged bubbles, but further study showed that this may not be the case. Higher magnification shows bubbles that were initially thought to have coalesced were simply attracted together and formed bubble clusters. The bubbles initially form in long chains, as seen in Figure 5(a). There are three common bubble formations seen. The first is a “planet”-like formation seen in Figure 5(b). The next two are variations on the planet cluster, and are the “comet”-like formation and the “cyclone”-like formation seen in Figures 5(c) and 5(d), respectively.

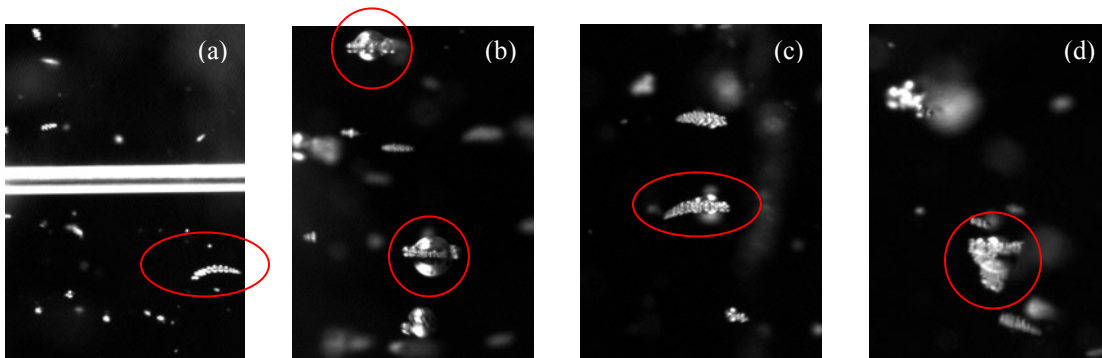


Figure 5: (a) Initial long chain bubble formation, (b) planet type bubble formation, (c) comet type bubble formation, (d) cyclone type bubble formation.

It is unclear as to how the larger bubbles form because actual bubble coalescence has not been observed. One possibility is that instead of coalescence, the gas within the smaller bubbles dissolves within the liquid and diffuses into a neighboring large bubble. It is also unclear what conditions result in release of some of the bubble clusters. There is the possibility that the bubble cluster's constant small motions become more erratic and it moves too far away from the pressure antinode, and buoyancy force overcomes the acoustic force. These topics will be addressed in further research.

Hydrophone Data

To determine the pressure in the acoustic chamber, and thus the average energy density of the system, a hydrophone can be utilized. Current readings show variable pressure throughout the chamber, which can change by as much as a factor of five based on position. However, it has also been observed that the readings at each position can change by a factor of two over time. So multiple runs at each location must be taken and averaged. Initial experiments have shown the average energy density to be lower than the 0.406 J/m^3 calculated to be the maximum energy density allowed for the bubbles to remain spherical, assuming a radius of $100 \text{ }\mu\text{m}$. Preliminary results indicate the energy density within the chamber when the transducer is operated at 0.55 MHz and 16 V peak-peak to be at least an order of magnitude lower than the desired maximum of 0.406 J/m^3 .

Conclusions and Future Work

It has been determined that operating conditions currently used (0.55 MHz , 16 V peak-peak) allow for bubble entrapment while still allowing for the spherical bubble assumption. The location of pressure antinodes has been modeled and verified through acquired visual data. Bubble movement, clustering, and coalescence have been investigated through modeling and data acquisition. Further work in these areas is needed to determine how coalescence comes about and what causes bubble release. Current modeling also needs to be adapted to include bubble-bubble interactions.

Acknowledgment

This work is sponsored by NASA Glenn Research Center under Grant NNC05GA29G.

References

1. Marston, P.L.; "Shape oscillation and static deformation of drops and bubbles driven by modulated radiation stresses – Theory;" *J. Acoust. Soc.*, **67** (1), 15-26 (1980).
2. Marston, P.L.; LoPorto-Arione, S.E.; Pullen, G.L.; "Quadrupole projection of the radiation pressure on a compressible sphere;" *J. Acoust. Soc.*, **69** (5), 1499-1501 (1981).
3. Yosioka, K.Y.; Kawasima, Y.; "Acoustic radiation force on a compressible sphere," *Acustica*, **5**, 167 (1955).
4. Lamb, H.; "Hydrodynamics," 6th edition, Cambridge University Press, London, (1932).
5. Rusinko, D.; "Design and Optimization of an Ultrasonic Standing Wave Chamber;" thesis, (2000).